

INVESTIGATION OF FLOW PARAMETERS AND NOISE OF SUBSONIC AND SUPERSONIC JETS USING RANS/ILES HIGH RESOLUTION METHOD

L.A. Benderskiy, D.A. Lyubimov
Central Institute of Aviation Motors, Russia

Leosun.Ben@gmail.com

DALyubimov@yandex.ru

Keywords: *effect of temperature, effect of chevron, supersonic and subsonic jets, noise, RANS/ILES*

Abstract

Flow parameters, turbulence characteristics and a noise for subsonic and supersonic jets from different nozzles have been calculated by high resolution RANS/ILES-method. The influence of chevrons (nozzles SMC001, SMC006) for subsonic cold jet with acoustic Mach 0.9 was considered. The effect of chevrons increases with increase their penetration. Chevrons reduce the noise at low and increase the noise at high frequencies. An influence of total temperature at the inlet of biconical nozzle for off-design supersonic jet with NPR=4.0 was studied. It is found that the temperature increase leads to a decrease in the length of a jet initial part due to more rapid closing of the jet mixing layers. Moreover, static pressure fluctuations in the mixing layer and noise in the jet near field are increased with jet temperature increase. A good agreement with the experimental data of other authors was obtained.

1 Introduction

The jet noise is one of the most important characteristics of the aircraft. Much effort is directed to study of ways to reduce it for example a study of microjet injection into mixed layer [1-3], a study of chevron geometry [4-6] and other. Experimental investigations of jet flows are complicated and usually difficult to get the whole range of flow characteristics in a single experiment. Therefore much effort [3, 7-12] is devoted to creation and perfection of

calculation methods of jet flow and noise. The simulation together with experiment can give more information for understanding the processes of noise generation and methods to reduce the jet noise.

There is the example [3] of subsonic jet noise calculating for model nozzle up to $St=10$ on the structured grid containing 23×10^6 cells. Additionally the microjet noise reduction was studied in work [3]. The noise of a supersonic jet from a chevron nozzle was predicted in [7]. All of these examples are based on LES-methods that show those methods are promising for calculating noise of turbulent jets. The main constraint is the computing power. For example, for calculating the jet flow together with the nozzle flow, it is necessary to resolve the boundary layer at the nozzle walls, which can be expensive for realistic Reynolds numbers. Estimations made in [9] talking about grid contained 40×10^9 cells. There are example [10] of calculation on grids of 400×10^6 cells. Calculations on this grid are quite expensive. However, even parameters of turbulence near the nozzle edge significantly differ from the experimental data for these calculations.

An alternative approach is to use a hybrid RANS/LES-methods [12, 13], where the flow near the walls is calculated using RANS and turbulence models, and the core flow is calculated by LES method. An additional increase in the method efficiency is achieved with applying high-resolution schemes for the calculation of flow parameters on cell faces [13]. This approach allows the use of much

coarser grid for the calculations and provides a good agreement with experiment [13, 14] even at high Reynolds numbers.

The purpose of this work is calculating flow parameters, turbulence characteristics and noise for subsonic and supersonic jets. Moreover, the effect of chevron for the subsonic jet noise and the effect of temperature on flow and noise in near field of supersonic jet was studied.

2 Numerical method

The method is based on Navier-Stokes equations describing the flow of a compressible gas. The transport equation for turbulence model is written in conservative form for curvilinear coordinate system. The grid lines coincide with the boundaries of computational domain, the nozzle surface and the flat plate. Hybrid RANS/ILES–method is used to solve equations. The RANS method is used near walls and ILES is used in the rest of the computational domain. The scheme viscosity performs a function of a subgrid scale (SGS) model. The Roe method was applied to calculate non-viscous flux on cell faces. The high resolution of this method is provided by using a monotone difference scheme MP9 [15] with upwind 9th-order approximation to calculate flow parameters on cell faces. This approach has been successfully used in [16]. Diffusion fluxes are calculated on cell faces with second-order approximation by central differences. The time discretization is made with second order by implicit scheme and with integration by double- time method. The Spalart–Allmarasa turbulence model [17] is used in RANS region. The WENO–5 scheme [15] is used to calculate convective flows on cell faces in the difference analog of turbulence model equation. In LES region, the Spalart–Allmarasa turbulence model is modified so that the turbulent viscosity is equated to zero. This is achieved by changing the distance dissipative term of turbulence model equation. The modified distance \tilde{d} is calculated by the formula:

$$\tilde{d} = \begin{cases} d, & d \leq C_{DES}\Delta_{MAX} \\ 10^{-6}L_{ref}, & d > C_{DES}\Delta_{MAX} \end{cases}$$

where d – the distance from the wall to the cell center, Δ_{MAX} – the maximum size of the cell, $C_{DES}=0.65$ and L_{ref} – characteristic dimension of the simulation.

This method has worked well in the calculation of sub- and supersonic jets from nozzles of different configurations [13, 14].

Noise calculations in far-field were performed using the aeroacoustic integrals (method FWH). Usually «retarded time stepping method» is used to calculate a noise from a Kirchhoff surface. However this method requires storing very large amounts of data. In this work «forward time stepping method» [11] was used. This is an alternative, more cost-effective and easy to implement method. The jet noise was calculated by averaging over outflow disks. This method proposed Shur et al. [8].

3 Simulations parameters

Calculations of subsonic jets were carried out on structured grids containing $(2.8\text{--}3.1)\times 10^6$ cells. Computational domain for subsonic jet from SMC000 nozzle is shown in Fig. 1a. The minimal longitudinal cell size and radial cell size near the nozzle edge are shown in Table 1. The grid contains 72 cells in the azimuthal direction. The number of grid cells for supersonic jets (Fig. 1b) is 4.5×10^6 and 72 cells are used in the azimuthal direction.

Table 1. Parameters of computational grids.

Nozzle	D_e , mm	Longitudinal cell size, $\Delta x/D_e$	Radial cell size, $\Delta r/D_e$
SMC000	50.8	0.016	0.0011
SMC001	52.8	0.016	0.0033
SMC006	47.7	0.017	0.0016
C-D	7.27	0.022	0.0038

Color-coded boundary conditions could be seen in Fig. 1: green – wall function/no-slip wall, red – the entrance to the nozzle, given the total pressure and temperature and the angle of the velocity vector. Orange – outlet boundary condition (parameters extrapolation). The computational grid step to the boundary of the computational domain increases to exclude

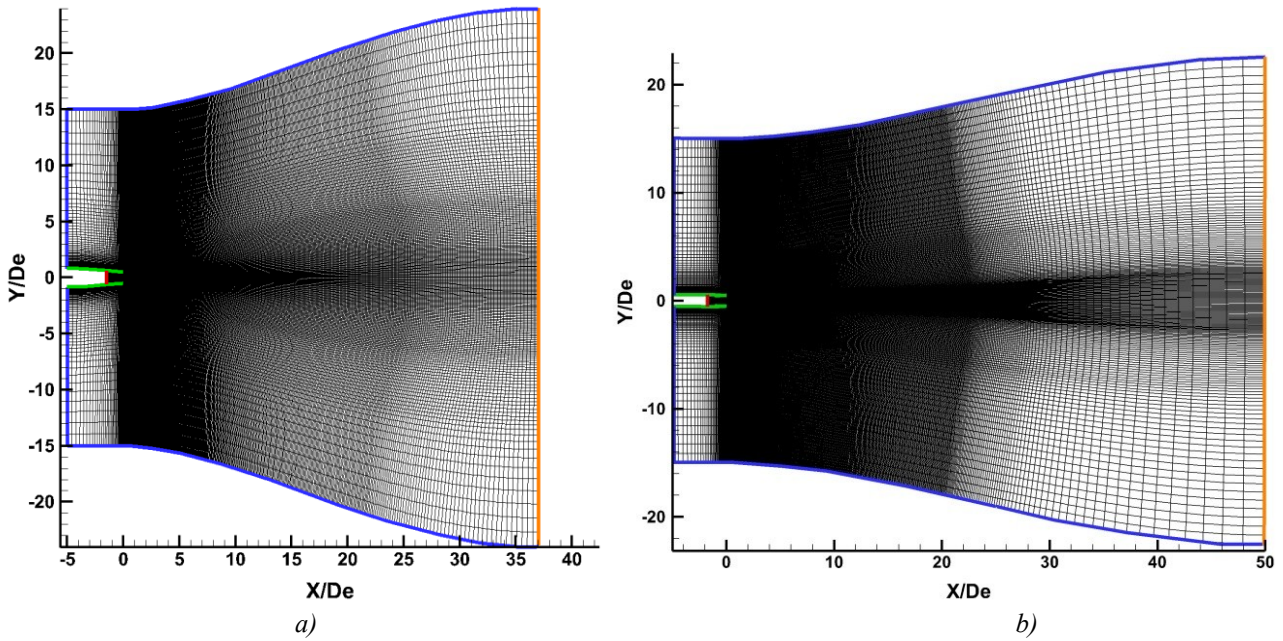


Fig. 1. Longitudinal section of computational grid: a) for SMC000, b) for C-D nozzle.

reflections from the outlet boundary. Blue – the far field asymptotic of the jet [18].

The conical nozzle geometry SMC000 and chevron nozzles geometry with penetration 5° SMC001 and 18.2° SMC006 close to the geometry described in [6]. The geometry of supersonic C-D nozzle is described in [19]. The geometry of studied nozzles is shown in Fig. 2.

The pressure and temperature in the ambient space are $P_{amb}=1 \times 10^5$ Pa and $T_{amb}=300$ K. Nozzle walls were considered as an adiabatic wall. Dimensionless time step and other simulation parameters are shown in Table 2, where NPR – nozzle pressure ratio, T_{0in} –

flow total temperature at the nozzle inlet and Re – Reynolds number calculated for parameters at the nozzle exit.

Table 2. Simulation parameters.

Nozzle	T_{in} , K	NPR	M_j	U_j , m/s	$Re \times 10^{-6}$	$\frac{\Delta t U_j}{D_e}$
SMC000	300	1.86	0.98	313	1.2	0.016
SMC001						0.015
SMC006						0.017
C-D	300	4.0	1.56	444	2.4	0.011
C-D	600			629	1.5	0.016

4 Simulations results

4.1 Subsonic jets

The following are calculations of cold subsonic jet with acoustic Mach number of 0.9 from nozzles SMC000, SMC001 and SMC006.

Fig. 3 shows isosurfaces of Q parameter $Q=0.5((S_{ij}S_{ij})^{0.5}-(\Omega_{ij}\Omega_{ij})^{0.5})$ where S_{ij} and Ω_{ij} are strain rate tensor and the vorticity. The small areal of the mixing layer with toroidal vortices regular structure is observed for the jet from the conical nozzle near the nozzle exit. This is caused by “numerical transition”. However, vortices are quickly destroyed and the flow becomes disordered – turbulent. There are compression of the mixing layer at the cut of chevron edge and expanding in the cut between chevrons. The effect of chevron increases with

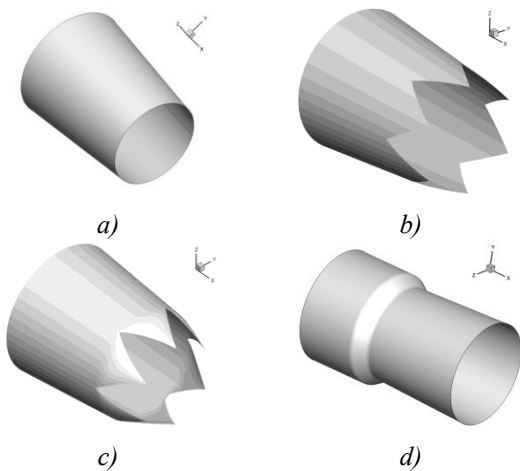


Fig. 2. Nozzles geometry: a) SMC000 b) SMC001, c) SMC006, d) C-D.

increasing chevron penetration. This is clearly seen in Fig. 4, which shows the contours of instantaneous static temperature. Moreover the mixing layer in the case of the nozzle SMC006 expanding faster than in the case of the nozzle SMC000 and SMC001. The consequence is the reduction of initial part of the jet from nozzle SMC006 on $1.5-2D_e$ in comparison with the jet from conical nozzle while the use of the nozzle SMC001 is not leading to significant changes. It corresponds to the experimental data [6] and [20] (Fig. 5).

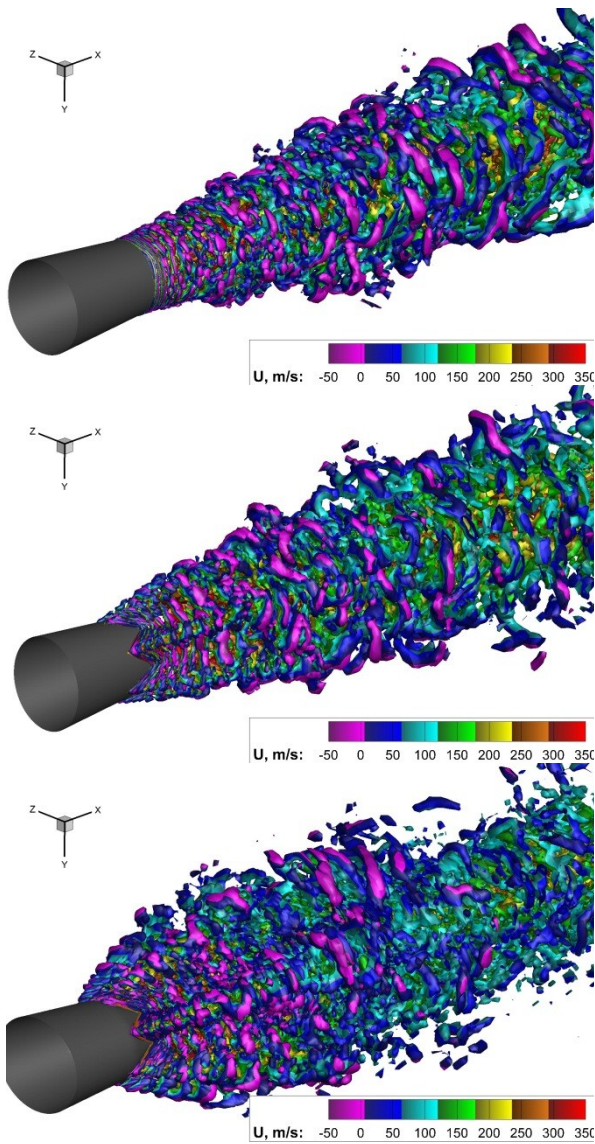


Fig. 3 Isosurfaces of Q parameter for jets from nozzles SMC000, SMC001 and SMC006 colored in longitudinal velocity.

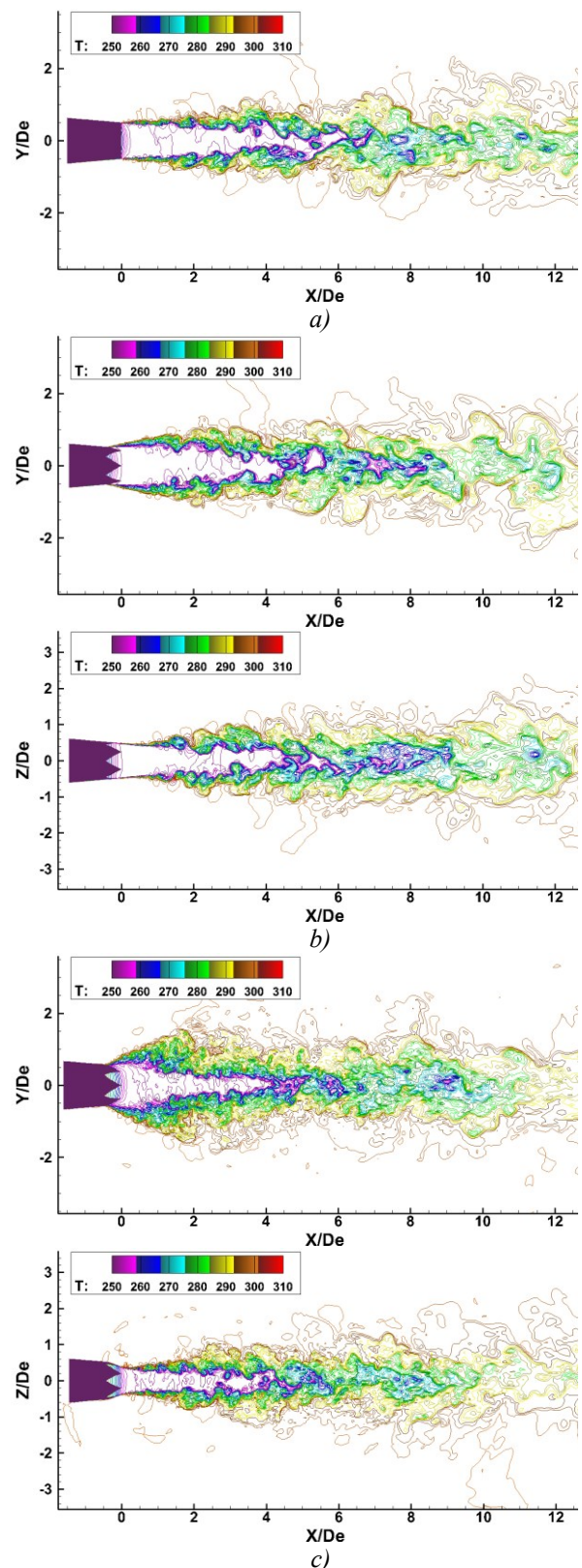


Fig. 4 Contours of instantaneous static temperature: a) SMC000, b) SMC001, c) SMC006.

Fig. 6 shows the pulsations of the longitudinal velocity in the mixing layer for the jet from the conical nozzle with the experimental data [21] and the maximum pulsations of longitudinal velocity for chevron nozzles with experimental data [12]. Seen that the magnitude of pulsations at small distance from the nozzle for jets from chevron nozzles is

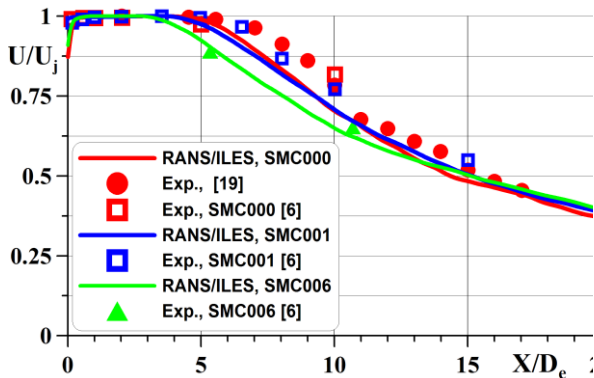


Fig. 5. Distributions of averaged longitudinal velocity along the jet axis.

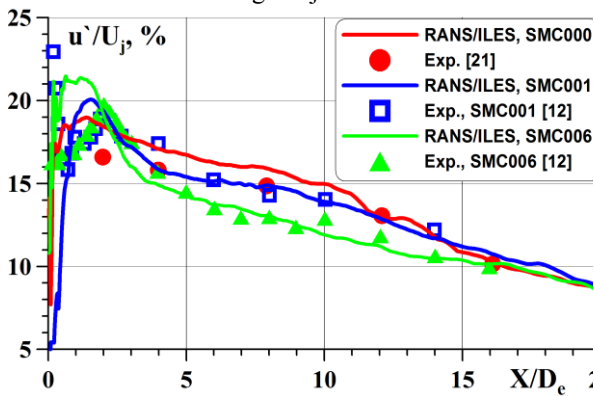


Fig. 6. Distributions of longitudinal velocity fluctuation at the mixing layer for the jet from SMC000 nozzle and the maximum pulsations of longitudinal velocity for chevron SMC001 and SMC006 nozzles.

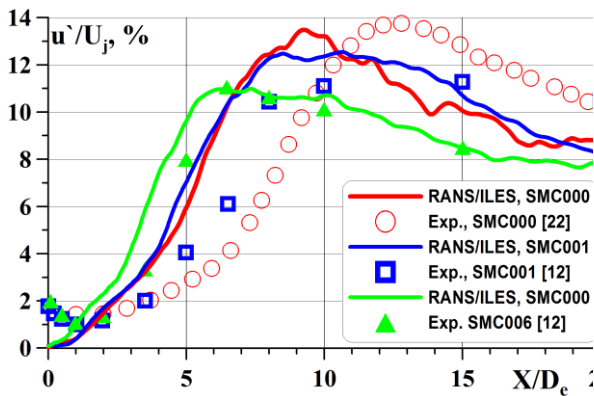


Fig. 7. Distributions of longitudinal velocity fluctuation along the jet axis.

greater than one for conical nozzle. This leads to the increase of the mixing layer thickness, which in turn reduces the pulsations of the longitudinal velocity at increasing distance from the nozzle. The maximum of longitudinal velocity publications along the jet axis for the jet from the SMC006 nozzle is less than ~20% compared with one for the jet from the conical nozzle (Fig. 7). In additions, experimental data [22] for the jet from conical nozzle and one [12] for jets from chevron nozzles are shown in Fig. 7. The greatest effect is achieved by using the SMC006 nozzle. It can be seen on the distribution of the longitudinal velocity fluctuations, averaged longitudinal velocity and contours of instantaneous static temperature.

The noise of subsonic jets was calculated at distance $R/D_e=50$ from the nozzle exit. The observation angle Θ is measured from the positive direction of the X-axis.

Fig. 8 shows the results of calculating the overall sound pressure level. The use of chevrons reduces noise at observation angles below 30° and increases at higher observation angles. It can also be seen in Fig. 9, which shows the OASPL difference of jets from chevron nozzle and jet from conical nozzle. The reasons for such dependence are seen on the 1/3-octave spectra for angles 30° (Fig. 10) and

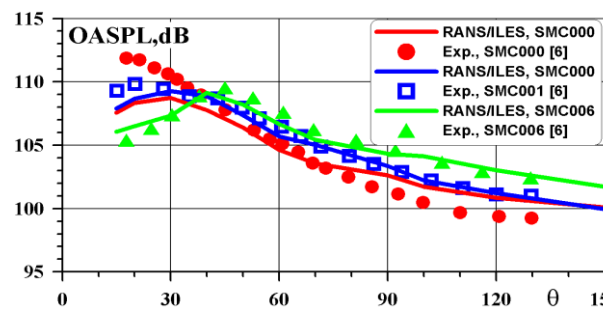


Fig. 8. Overall sound pressure level of jets noise at the far field.

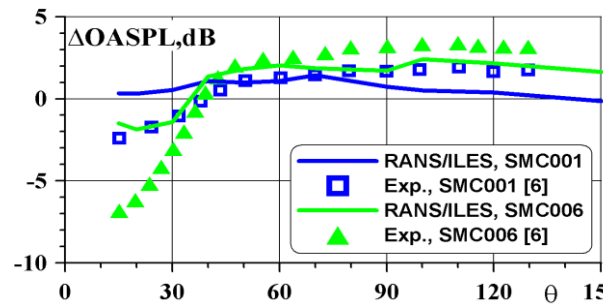


Fig. 9. OASPL difference of jets from chevron nozzle and jet from conical nozzle.

90° (Fig. 11). The use of chevrons reduces peak noise at frequencies $St = 0.2$ to 4dB for the jet from the nozzle SMC006 at observation angle of 30°. The slight decrease in noise at low frequencies $St < 0.6$ and the increase to 5 dB (SMC006) noise at high frequencies $St > 1$ are observed at angle of 90°.

In additions in Fig. 8-11 shows the experimental data from [6]. OASPL (Fig. 8) is well agreement with the experimental data within 0.5-1.5dB for observation angles of 30° – 130°. Spectrum of jets from conical and SMC001 nozzles correspond to experiments within 0.5 to 2.5 dB at $St=0.06-4$ (Fig. 10-11) and for chevron SMC006 nozzle within 0.5-2dB at $St=0.06-10$

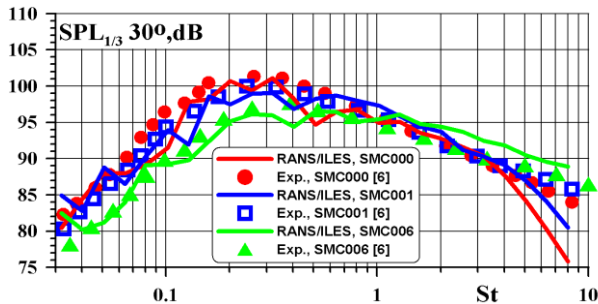


Fig. 10. 1/3-octave noise spectra of jets for observation angle of 30°.

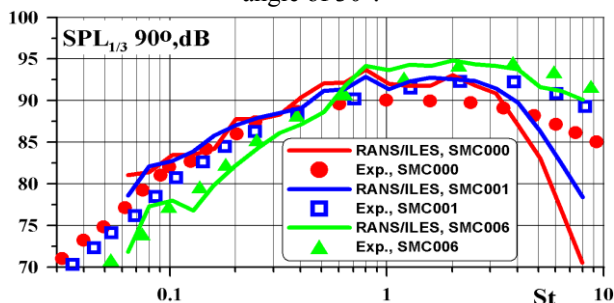


Fig. 11. 1/3-octave noise spectra of jets for observation angle of 90°.

4.2 Supersonic jets

The following are the results of calculations off-design supersonic cold $T_{in}=300K$ and hot $T_{in} = 600K$ jets from the C-D nozzle at $NPR = 4.0$.

Fig. 12 shows isosurfaces of Q parameter. The flow near the nozzle exit has the regular structure and it becomes turbulent at approximately $1D_e$ from nozzle exit.

Fig. 13 shows the field of $\log(|grad\rho|)$. It can be seen that the hot jet has a larger angle of the mixing layer expansion than the cold jet.

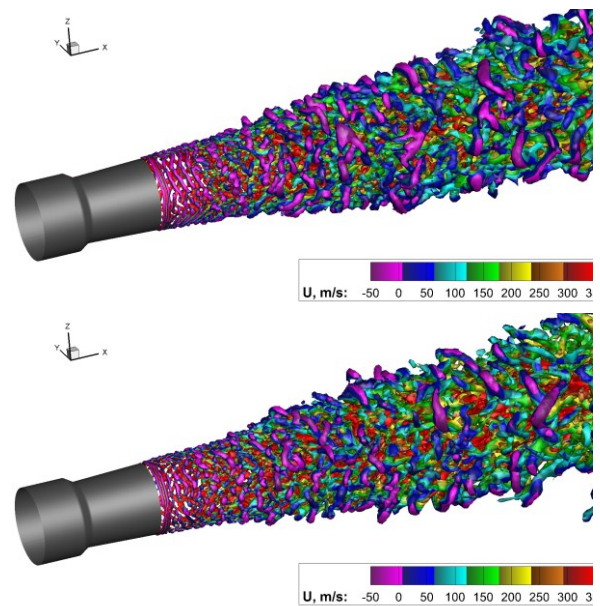


Fig. 12. Isosurfaces of Q parameter for cold (top) and hot (bottom) jets.

The system of shocks and Mach disk at the jet axis was resolved. The greater angle extension of the mixing layer in the hot jet leads to a decrease in the length of the jet initial part (Fig. 14). This is due to increased levels of pulsations in the mixing layer of hot jet (Fig. 15). There is a "numerical transition" for both jets at $X/D_e \approx 1$, which leads to overestimation of the longitudinal velocity fluctuations. Additionally Fig. 14 demonstrates the results of calculations [19], where the calculations were performed using the ILES, based on the solution of the Euler equations. The grid in [19] containing 66×10^6 tetrahedral cells. The boundary layer in the calculations [19] in the nozzle was missing, so the evolution of the mixing layer along the jet is different from that which was observed in calculating the present RANS/ILES-method.

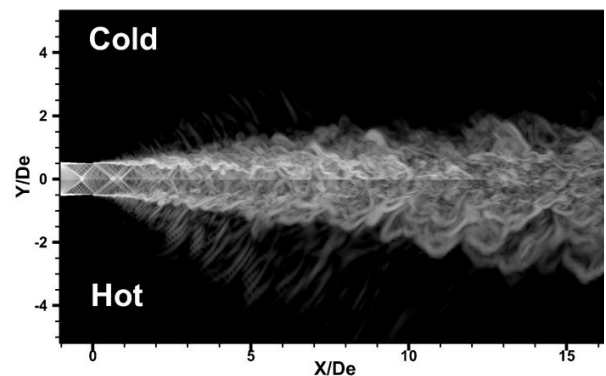


Fig. 13. The field of $\log(|grad\rho|)$ for cold and hot jets.

Fig. 14 illustrates this at the distribution of the averaged longitudinal velocity by the slightly different shocks structure. Fig. 15 also shows the data of the experiment [21], which studied the jet of the Laval nozzle at NPR = 3.05.

The static pressure fluctuations in the mixing layer (Fig 16) were obtained in the calculations. The level of fluctuations in the hot jet higher than one in cold jet approximately by 20% at $X/D_e=2-8$ and close to pulsations in cold jet at $X/D_e>10$. Additionally, in Fig. 16 shows the experimental data for subsonic jet [23].

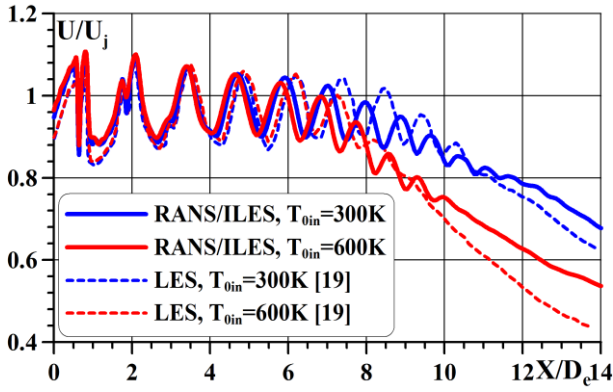


Fig. 14. Distributions of the averaged longitudinal velocity along jet axis.

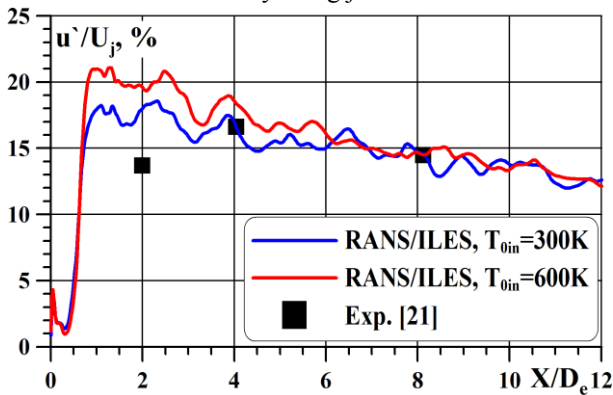


Fig. 15. The distribution of the longitudinal velocity fluctuations at the lip line.

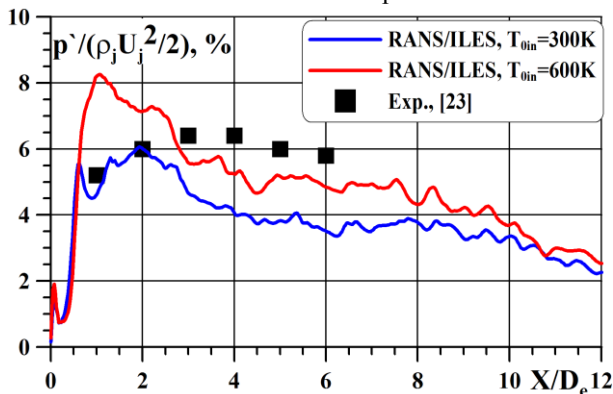


Fig. 16. The distribution of the static pressure fluctuations at the lip line.

Fig. 17 shows the distributions of OASPL in the near field of jets at the line at angle of 9.5° to the positive direction of the X-axis, and starting from the point $(0, 2D_e)$. It can be seen that the hot jet has a maximum noise level at $X/D_e=5$. The noise of the hot jet by 5-7 dB higher than one for cold jet at $X/D_e>2$, and it decreases monotonically for $X/D_e>10$. It may be noted that the increasing noise in near field for hot jet in comparison with cold jet are observed against the increasing of static pressure fluctuations in the mixing layer. Fig. 17 also shows the experimental data of noise from cold supersonic jet [24]. This calculation is in satisfactory agreement with experimental data.

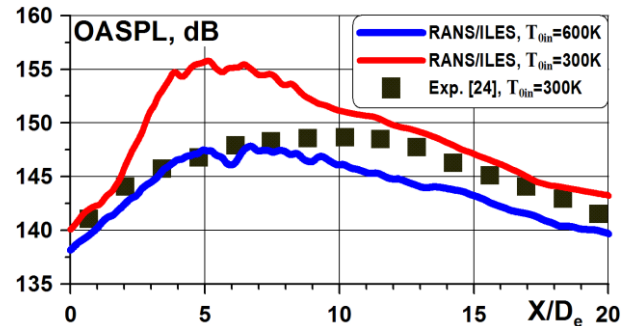


Fig. 17. Distributions of supersonic jet noise OASPL in near field.

5 Conclusions

Overall, the results indicate that the presented high resolution RANS/ILES-method on grids contains $(2.8-4.5) \times 10^6$ cells allows to get a good accuracy of the calculation of the averaged flow parameters, turbulence and acoustic characteristics for subsonic and supersonic jets from nozzles of various types.

It was found that the effect of chevrons is proportional to the chevron penetration. Using chevrons intensifies the mixing of the jet and reduces the length of the jet initial part. The length of the initial part of the jet from SMC006 nozzle is decreased by $1.5-2D_e$ in comparison with the jet from conical nozzle SMC000. The use of chevrons reduces low-frequency noise and increases noise at high frequencies. So reduction of low frequency noise on the observation angle of 30° was 4dB and the gain of high frequency noise by up to 5 dB for the observation angle of 90° for the jet from SMC006 nozzle.

The effect of temperature on flow parameters and turbulence was studied for supersonic jets. It has been established that the increase in jet temperature leads to an increase in pulsations of the longitudinal velocity in the mixing layer, the increase of the expansion angle of the mixing layer and the decrease in the length of the jet initial part. Increasing the jet total temperature with 300K to 600K increases static pressure fluctuation in the mixing layer and increases the overall noise level in the near field of the jet by 5-7dB at $X/D_e > 2$.

Acknowledgments

The work was supported by RFBR (grant number 12-08-00951-a).

References

- [1] K.B.M.Q. Zaman, G.G. Podboy Effect of microjet injection on supersonic jet noise. *AIAA*, 2010-4022, 2010.
- [2] D. Munday, N. Heeb, E. Gutmark J. Liu, K. Kailasanath Fluidic Injection for Noise Reduction of a Supersonic Jet from a practical C-D nozzle. *AIAA*, 2010-4028, 2010.
- [3] M.L. Shur, P.R. Spalart, M. Kh. Strelets LES-based evaluation of a microjet noise reduction concept in static and flight conditions. *Journal of Sound and Vibration*, Vol. 330, pp. 4083–4097, 2011.
- [4] B. Henderson, J. Bridges An MDOE Investigation of Chevrons for Supersonic Jet Noise Reduction. *AIAA*, 2010-3926, 2010.
- [5] P.S. Tide, K. Srinivasan Effect of chevron count and penetration on the acoustic characteristics of chevron nozzles. *Applied Acoustics*, Vol. 71, pp. 201–220, 2010.
- [6] J. Bridges, Clifford A. Brown Parametric Testing of Chevrons on Single Flow Hot Jets. *AIAA*, 2004–2824, 2004.
- [7] G. A. Bres, J.W. Nichols, S.K. Lele, F.E. Ham, R.H. Schlinker, R. A. Reba, J.C. Simonich Unstructured Large Eddy Simulation of a Hot Supersonic Over-Expanded Jet with Chevrons. *AIAA*, 2012-2213, 2012.
- [8] M L. Shur, P. R. Spalart, M. Kh. Strelets Noise prediction for increasingly complex jets. Part I: Methods and tests. *International Journal of Aeroacoustics*, Vol. 4, No. 3&4, pp. 213-246, 2005.
- [9] Uzun A., Hussain, M.Y. Simulation of Noise Generation in Near-Nozzle Region of a Chevron Nozzle Jet. *AIAA J.*, Vol. 47, No. 8, pp. 1793-1810, 2009.
- [10] Uzun A., Hussaini M.S. High-Fidelity Numerical Simulation of a Round Nozzle Jet Flow. *AIAA*, 2010-4016. 2010.
- [11] Ozoruk Y., Long L.N. Computation of Sound Radiating from Engine Inlets. *AIAA J.*, Vol. 34, No. 5, p. 864, 1996.
- [12] Xia H., Paul G., Tucker P.G., Eastwood S. Towards Jet Flow LES of Conceptual Nozzles for Acoustic Predictions. *AIAA*, 2008–10, 2008.
- [13] Lyubimov D.A. Development and application of a high-resolution technique for jet flow computation using large eddy simulation. *High Temperature*, Vol. 50, No. 3, pp. 450-466., 2012.
- [14] Bendersky L. A., Lyubimov D.A. Using large-eddy simulation method for the research influence of total flow parameters at the nozzle inlet and off-design conditions on the flow and turbulence characteristics in a supersonic jet flowing out of biconical nozzles flow. *XVI International Conference on the Methods of Aerophysical Research*, Kazan, Russia, Vol. 1, pp. 47-48, 2012.
- [15] Suresh A., Huynh H. T. Accurate Monotonicity–Preserving Schemes with Runge-Kutta Time Stepping. *J. Comput. Phys*, Vol. 136, No. 1, p. 83, 1997.
- [16] Grinstein F.F., Margolin L.G., Rider W.J. *Implicit Large Eddy Simulation: Computing Turbulent Fluid Dynamics*. Cambridge University Press, 2007.
- [17] Spalart P.R., Allmaras S.R. A One-Equation Turbulence Model for Aerodynamic Flows. *La Recherche Aerospaciale*, No. 1, p. 5, 1994.
- [18] L.D. Landau, E.M. Lifshitz. *Fluid Mechanics*. Vol. 6, 2nd edition, Butterworth-Heinemann, 1987.
- [19] Liu, J., Kailasanath K., Munday, D., Nick, H., Gutmark, E. Large-Eddy Simulation of a supersonic heated jet. *AIAA*, 2011-2884, 2011.
- [20] Lau J.C., Morris P.J., Fisher M.J. Measurements in Subsonic and Supersonic Free Jets Using a Laser Velocimeter. *J. Fluid Mech.*, Vol. 93, No. 1, p. 1, 1979.
- [21] Lau J.C. Effects of exit Mach number and temperature on mean-flow and turbulence characteristics in round jets. *J. Fluid Mech.*, Vol. 105, pp. 193-218, 1981.
- [22] J. Bridges, Wernet M.R. Establishing Consensus Turbulence Statistics for Hot Subsonic Jets. *AIAA*, 2010-3751, 2010.
- [23] Jones B.G., Adrian R.J., Nithianandan C.K., Plachon H.P. Spectra of Turbulent Static Pressure Fluctuations in Jet Mixing Layers. *AIAA J.*, Vol. 17, No 5, p. 449, 1979.
- [24] J. Liu, A. Corrigan, K. Kailasanath, R. Ramammurti, N. Heeb, D. Munday, E. Gutmark Impact of Deck and Jet Blast Deflector on the Flow and Acoustic Properties of Imperfectly Expanded Supersonic Jets. *AIAA*, 2013-0323, 2013.

Copyright Statement

The authors confirm that they, and/or their company or organization, hold copyright on all of the original material included in this paper. The authors also confirm that they have obtained permission, from the copyright holder of any third party material included in this paper, to publish it as part of their paper. The authors confirm that they give permission, or have obtained permission from the copyright holder of this paper, for the publication and distribution of this paper as part of the ICAS 2014 proceedings or as individual off-prints from the proceedings.